PROCEEDINGS OF SCIENCE

Simultaneous Photoproduction Of Neutral And Charged Pions On The Deuteron At ELPH

Takatsugu Ishikawa*, **Akihiko Nakamura, Hisako Fujimura, Ryo Hashimoto, Qinghua He, Shun Kaida, Manabu Miyabe, Norihito Muramatsu, Hajime Shimizu, Koutaku Suzuki, Yusuke Tschikawa, Hirohito Yamazaki, Ryuji Yamazaki**
Research Center for Electron Photon Science (ELPH), Tohoku University, Sendai 982-0826, Japan

Shin'ichi Masumoto, Yuki Obara

Department of Physics, University of Tokyo, Tokyo 113-0033, Japann

Kazushige Maeda

Department of Physics, Tohoku University, Sendai 980-8578, Japan

Kyoichiro Ozawa
Institute of Particle and Nuclear Studies, KEK, Tsukuba 305-0801, Japan

for the FOREST collaboration
E-mail: ishikawa@lns.tohoku.ac.jp

We have measured the cross sections for $\pi^0\pi^\pm$ photoproduction on the nucleon in the deuteron with an electromagnetic calorimeter system, FOREST, at the Research Center for Electron Photon Science, Tohoku University, Japan. The incident photon energy ranges from 570 to 1150 MeV, corresponding to the γN center of mass, $W_{\gamma N}$, from 1400 to 1750 MeV. The baryon resonances coupling to $\rho^+ n$ and $\rho^- p$ are observed as intermediate states together with Δ-Kroll-Ruderman background components. The angular distributions for the produced ρ^+ and ρ^- mesons are convex downward and upward at high energies ($W_{\gamma N} \sim 1720$ MeV), respectively.

The 26th International Nuclear Physics Conference
11-16 September, 2016
Adelaide, Australia

*Speaker.

PoS(INPC2016)267

1. Introduction

Baryon spectroscopy is an important subject in the non-perturbative domain of the quantum chromodynamics (QCD). Highly excited nucleon and delta resonances have a large branching ratio of $\pi\pi N$ decay modes and hardly couple to πN, and they have not been well investigated via elastic πN scattering. Double π photoproduction is expected to be an alternative probe to study them. So far, only MAMI experiments reported the cross sections for $\pi^0\pi^+$ photoproduction on the proton [1]. These experiments cover the baryon masses below 1550 MeV because the maximum incident photon energy is 820 MeV. The $\gamma p \to \pi^0\pi^+ n$ and $\gamma n \to \pi^0\pi^- p$ reactions on the proton and deuteron were measured at the Research Center for Electron Photon Science (ELPH), Tohoku University for the photon energies below 1150 MeV [2, 3] corresponding to the baryon masses below 1750 MeV.

2. Experiment

Bremsstrahlung photons were used as a beam, being generated with a thin carbon wire inserting into the 1200 and 920 MeV circulating electrons in a synchrotron called STretcher Booster (STB) ring [4]. Each photon was energy-tagged measuring the momentum of the corresponding post-bremsstrahlung electron with a photon tagging counter, STB-Tagger II, in a bending magnet of the ring [2]. The targets used were liquid hydrogen and liquid deuterium with a thickness of 45 mm [5]. All the final-state particles, $\pi^\pm$, two photons from the π^0 decay, n and p, are detected with an electromagnetic calorimeter complex, FOREST [6]. FOREST consists of three different EM calorimeters: the forward, central, and backward calorimeters consisting of 192 pure CsI crystals, 252 lead scintillating fiber modules, and 62 lead glass Cherenkov counters, respectively. The typical energy resolutions of the forward, central, and backward calorimeters are 3%, 7%, and 5% for 1-GeV photons, respectively. A plastic scintillator (PS) hodoscope is placed in front of each calorimeter to identify the charged particles. The solid angle of FOREST is approximately 88% in total. The typical tagging rates were 20 and 2.8 MHz for 1200 and 920 MeV circulating electron modes, which covered the tagging energies of 740–1150 and 570–890 MeV, respectively.

3. Analysis

Events detected in the final state containing two neutral particles, a charged particle, and a nucleon were selected. A neutral pion was identified via its decay into $\gamma\gamma$, where the time difference between two neutral clusters was required to be less than $3\sigma_t$, where σ_t denotes the time resolution for the difference depending on the modules and their measured energies for the two clusters. Fig. 1(a) shows the $\gamma\gamma$ invariant mass distribution. A clear peak corresponding to the neutral pion was observed, and the events in which the mass from 50 to 220 MeV were selected as neutral-pion production.

The events containing the charged pion and proton were selected utilizing ΔE-E correlation between the hodoscope and corresponding calorimeter. Fig. 1(b) shows the typical ΔE-E correlation between the forward hodoscope and calorimeter. Two loci corresponding to the charged pion and proton are observed clearly. The events in the depicted region were selected as charged-pion

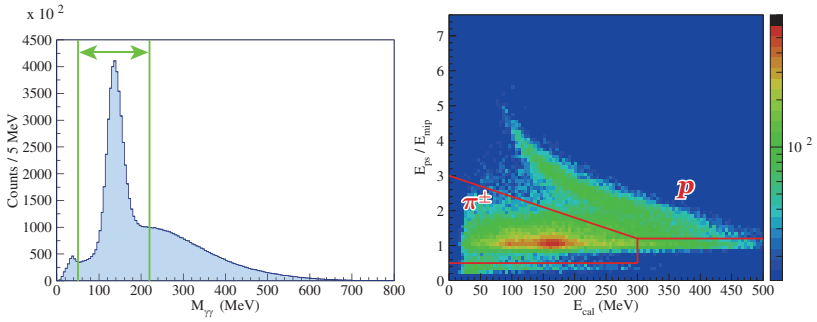

Figure 1: (a) $\gamma\gamma$ invariant mass distribution. The events in which the mass from 50 to 220 MeV are selected as neutral-pion production. (b) ΔE-E correlation between the forward hodoscope and calorimeter. The events in the depicted region are selected as charged-pion and proton production.

and proton production. The events containing the neutron was selected utilizing the time delay with respect to the average timing of the two photon detection. Fig. 2(a) shows the time delay of a cluster from the two-photon timing. Bumps corresponding to the neutron are observed clearly both for the forward and central calorimeters. Events in which the time delay larger than 1.5 and 1.0 ns were selected as neutron production for the forward and central calorimeters, respectively.

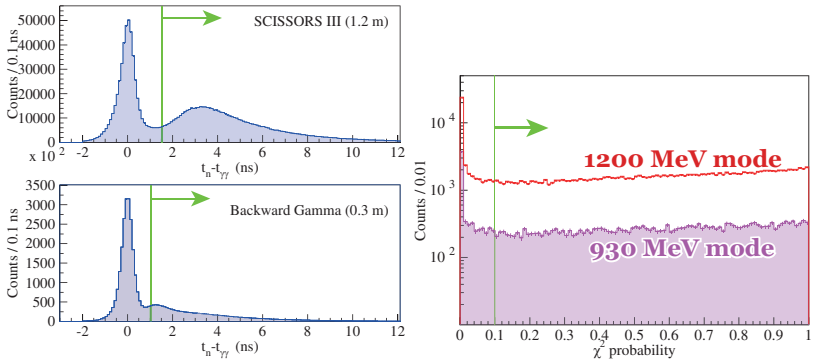

Figure 2: (a) Time delay of a cluster from the two-photon timing. Events in which the time delay larger than 1.5 and 1.0 ns are selected as neutron production for the forward and central calorimeters. The upper panel shows those for the forward calorimeter (SCISSORS III), and the lower shows those for the central calorimeter (Backward Gamma). (b) χ^2 probability distribution of the 4C kinematic fit for the hydrogen target. Events in which the χ^2 probability is higher than 0.1 are selected for the $\gamma p \to \pi^0\pi^+ n$ reaction.

A kinematic fit with four constraints (4C) was applied for the further event selection of the $\gamma N' \to \pi^0\pi^{\pm}N$ reaction. The kinematic variables in the fit were the incident photon energy, and the three-momentum of the four final-state particles for the hydrogen target. Since the velocity of the charged pion is close to the speed of light, the absolute value of the momentum was treated as unmeasured. The required constraints were energy and three-momentum conservation between the initial and final states and the $\gamma\gamma$ invariant masses (the neutral-pion rest mass, m_{π^0}). The five constraints and a unmeasured variable give four constraints in total. Events in which the χ^2 probability was higher than 0.1 were selected. Fig. 2(b) shows the χ^2 probability distribution of the 4C

kinematic fit. Because accidental coincidence events exist between the photon-tagging counter and FOREST, sideband background subtraction was performed. The (x,y,z) components of the Fermi motion were added as kinematic variables for the deuterium target, and they were assumed to be measured with a resolution of 40 MeV$/c$.

4. Results for the hydrogen target

In this section, the results for the hydrogen target are given at first. The total cross section was obtained as a function of E_γ. Here, the detector acceptance correction and neutron efficiency correction were made. The acceptance was estimated for each $M_{\pi^0\pi^+}$ and $M_{\pi^0 n}$ bin using a Monte Carlo simulation based on Geant4 [7]. The detection efficiency for the neutron was estimated using the real data, and it was corrected artificially in the simulation. Figure 3 shows the total cross section as a function of E_γ. The obtained total cross sections are consistent for two circulating electron energy modes, and with the previous Mainz data [1] obtained for $E_\gamma < 820$ MeV. Although they are consistent with the 2-PION MAID calculation [8] below the incident energy of 750 MeV, they are much smaller than the calculation results above 750 MeV.

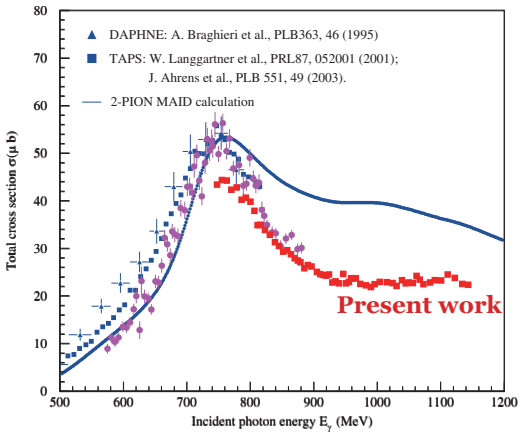

Figure 3: Total cross section as a function of E_γ. The filled circles (magenta) and filled boxes (red) show the present work, and are compared with the previous Mainz data [1] and 2-PION MAID calculation [8].

To investigate the reaction mechanism, the correlation between two invariant masses for the two final-state particles of three. Fig. 4 shows the typical correlations between $\pi^0\pi^+$, $\pi^+ n$, and $\pi^0 n$ invariant masses. The event concentration at a $\pi^0 n$ invariant mass of the Δ mass was clearly observed, suggesting sequential π^+ and π^0 emission exists called Δ-Kroll-Ruderman term, namely the $\gamma p \to \pi^+\Delta^0$ reaction, in which the contact term is dominant, with the successive $\Delta^0 \to \pi^0 n$ decay. Fig, 5 shows the $\pi^0\pi^+$, $\pi^+ n$, and $\pi^0 n$ invariant mass distributions. Although a consistent result was obtained at $W \sim 1520$ MeV where the $D_{13}(1520)$ nucleon resonance is dominant, the calculation was overestimated approximately twice at $W \sim 1680$ MeV. More stronger peak is observed in the $\pi^0 n$ invariant masses, suggesting the contribution form the Δ-Kroll-Ruderman term is larger.

An enhancement in the higher $\pi^0\pi^+$ invariant mass is also observed, suggesting the ρ^+ meson is produced directly or from the decay of intermediate baryon resonances. The angular distribution

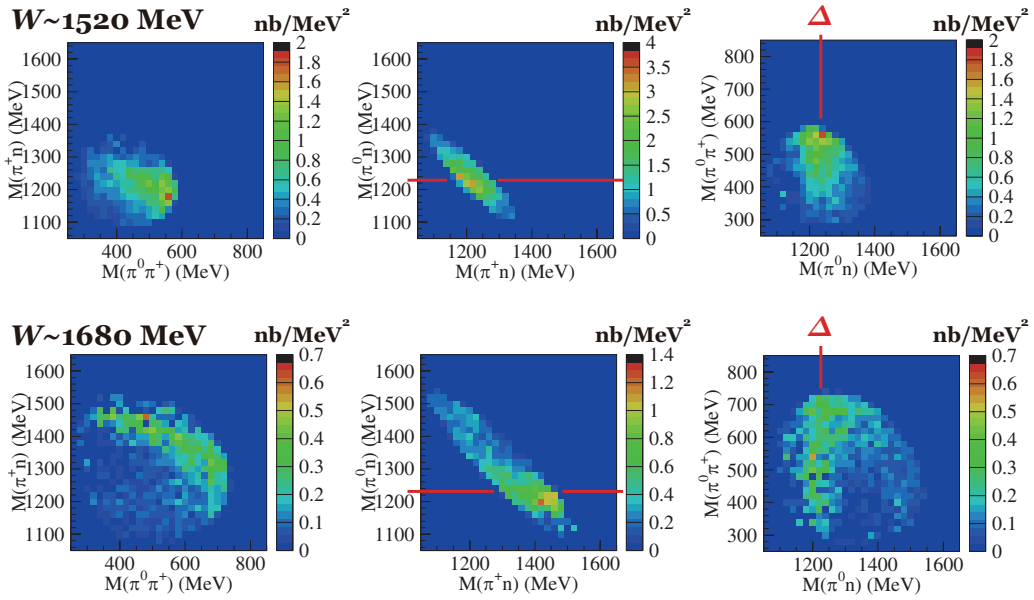

Figure 4: Correlations between $\pi^0\pi^+$, π^+n, and π^0n invariant masses ($M_{\pi^0\pi^+}$, M_{π^+n}, and M_{π^0n}). The upper and lower panels shows the correlations for $W \sim 1520$ and 1680 MeV, respectively. The left, central, and right panels show the correlations M_{π^+n} vs $M_{\pi^0\pi^+}$, M_{π^0n} vs M_{π^+n}, and $M_{\pi^0\pi^+}$ vs M_{π^0n}. The event concentration at a M_{π^0n} of the Δ mass is clearly observed in both W.

of the emitted ρ^+ meson was obtained. Here, evens in which the $\pi^0\pi^+$ invariant mass was higher than 650 MeV were assumed that the ρ^+ meson was produced. Fig. 6 shows the typical differential cross section of ρ^+ production. The angular distributions were convex downward, suggesting that a baryon resonance with higher J exists.

5. Results for the deuterium target

In this section, the results for the deuterium target are given. The total cross section was obtained as a function of E_γ in the similar way to the hydrogen target. Figure 7 shows the total cross section as a function of E_γ. Both the total cross sections are smaller at $W \sim 1520$ MeV thatn that for the $\gamma p \to \pi^0\pi^+n$ reaction for the hydrogen target. In this energy region, the $\gamma n' \to \pi^0\pi^- p$ reaction have higher cross section than the $\gamma p' \to \pi^0\pi^+n$ for the deuterium target. At high energies, the $\gamma n' \to \pi^0\pi^- p$ reaction have lower cross section than the $\gamma p' \to \pi^0\pi^+n$, which is almost the same as the $\gamma p' \to \pi^0\pi^+n$ for the hydrogen target.

To investigate the reaction mechanism, the correlation between two invariant masses for the two final-state particles of three. Fig. 8 shows the typical correlations between $\pi^0\pi^+$, $\pi^\pm N$, and π^0N invariant masses. The event concentration at a π^0N invariant mass of the Δ mass was also clearly observed, suggesting sequential $\pi^\pm$ and π^0 emission (Δ-Kroll-Ruderman term) exists.

An enhancement in the higher $\pi^0\pi^\pm$ invariant mass is also observed, suggesting the $\rho^\pm$ meson is produced. The locus corresponding to the ρ^- production seems weaker than that to the ρ^+ production. The angular distribution of the emitted $\rho^\pm$ meson was obtained, where evens in which

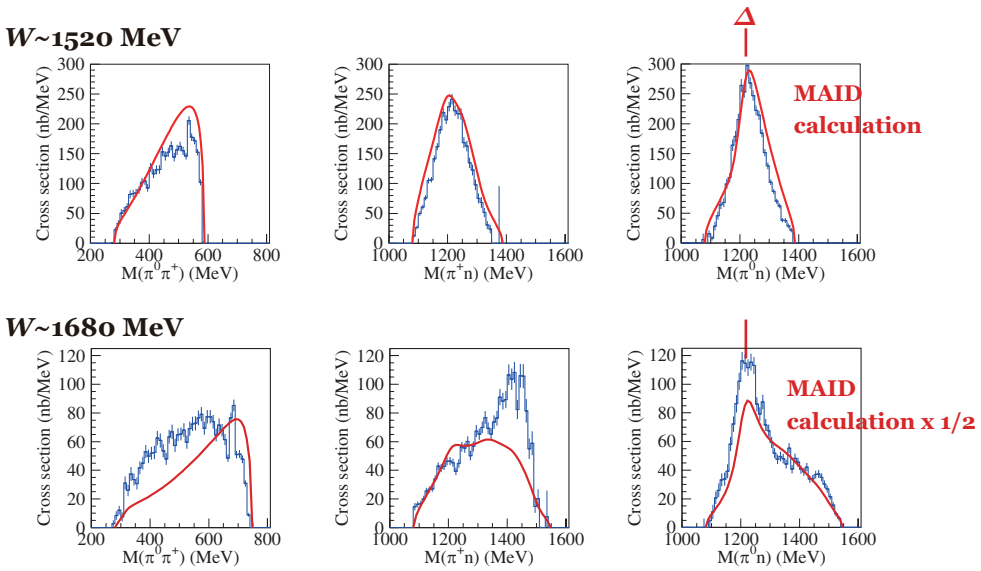

Figure 5: $\pi^0\pi^+$, π^+n, and π^0n invariant mass distributions. The upper and lower panels shows the correlations for $W \sim 1520$ and 1680 MeV, respectively. The curves (red) show the 2-PION MAID calculation, At $W = 1680$ MeV, the calculation is compared with the real data after dividing by 2.

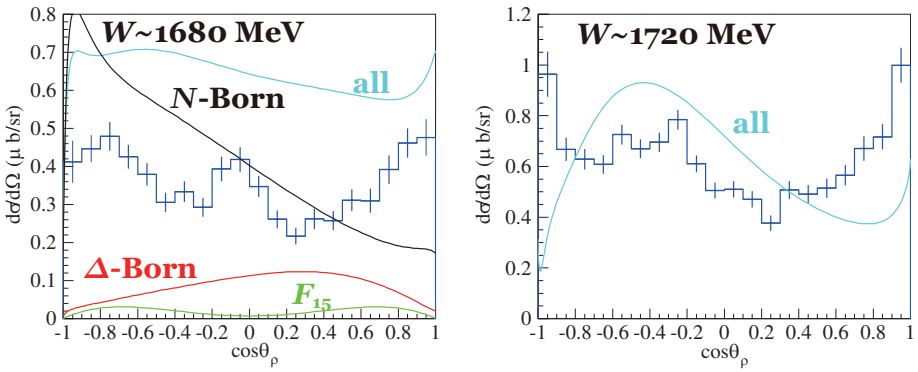

Figure 6: Differential cross section of ρ^+ production. Evens in which the $\pi^0\pi^+$ invariant mass is higher than 650 MeV are assumed that the ρ^+ meson is produced. The left panel shows that for $W \sim 1680$ MeV, and the right shows that for $W \sim 1720$ MeV. The curves show the 2-PION MAID calculation results; the cyan curves show the sum of all the components, and others show a corresponding component to the description in the panel.

the $\pi^0\pi^\pm$ invariant mass was higher than 650 MeV were assumed that the $\rho^\pm$ meson was produced. Fig. 9 shows the typical differential cross section of $\rho^\pm$ production. The angular distributions were also convex downward for the $\gamma p' \to \pi^0\pi^+n$ reaction, suggesting that a baryon resonance with higher J exists. And the angular distributions were also convex upward for the $\gamma p' \to \pi^0\pi^+n$ reaction, suggesting that a baryon resonance with $J = 3$ exists.

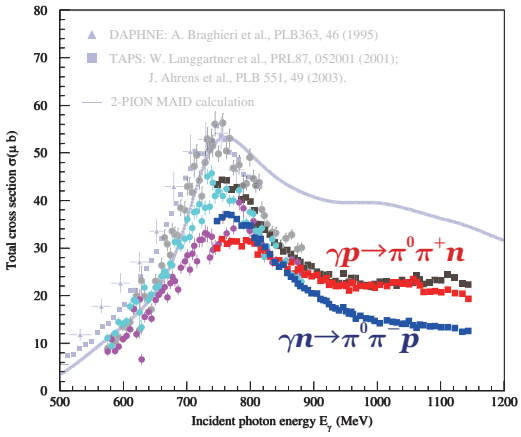

Figure 7: Total cross section as a function of E_γ. The filled circles (magenta) and filled boxes (red) show the $\gamma p' \to \pi^0\pi^+ n$ results, and the filled circles (cyan) and filled boxes (blue) show the $\gamma p' \to \pi^0\pi^- p$ results. The data are compared with the hydrogen results and calculation.

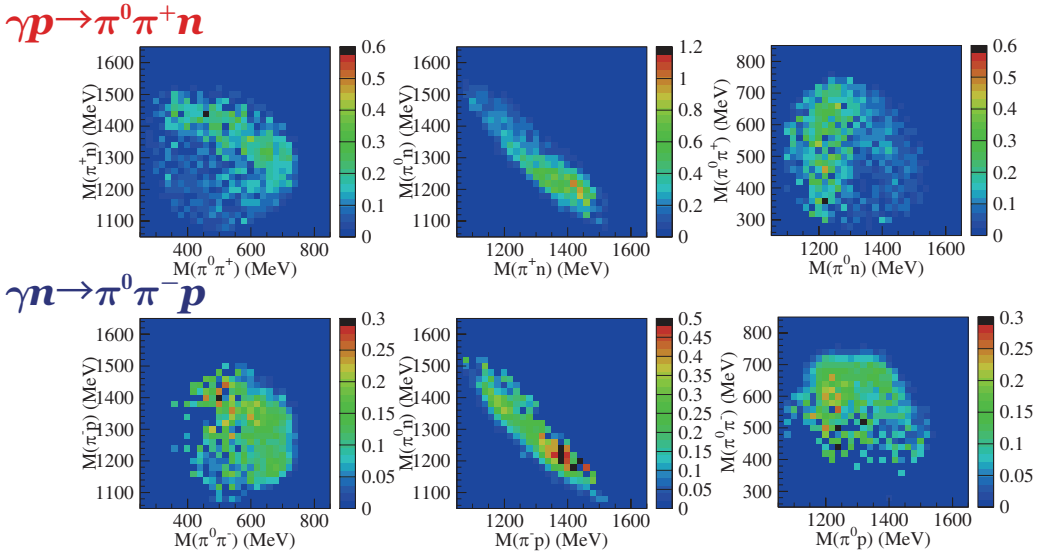

Figure 8: Correlations between $\pi^0\pi^\pm$, $\pi^p mN$, and $\pi^0 N$ invariant masses ($M_{\pi^0\pi^\pm}$, $M_{\pi^p mN}$, and $M_{\pi^0 N}$). The upper and lower panels shows the correlations for the $\gamma p' \to \pi^0\pi^+ n$ and $\gamma n' \to \pi^0\pi^- p$ reactions. The left, central, and right panels show the correlations $M_{\pi^\pm N}$ vs $M_{\pi^0\pi^\pm}$, $M_{\pi^0 N}$ vs $M_{\pi^\pm N}$, and $M_{\pi^0\pi^+}$ vs $M_{\pi^0 N}$.

6. Summary

We measured the cross sections for $\pi^0\pi^\pm$ photoproduction on the nucleon with FOREST electromagnetic calorimeter at ELPH. The incident photon energy ranged from 570 to 1150 MeV, corresponding to the γN center of mass from 1400 to 1750 MeV. The baryon resonances coupling to $\rho^+ n$ and $\rho^- p$ were observed as intermediate states together with Δ-Kroll-Ruderman background components. The angular distributions for the produced ρ^+ and ρ^- mesons were convex downward

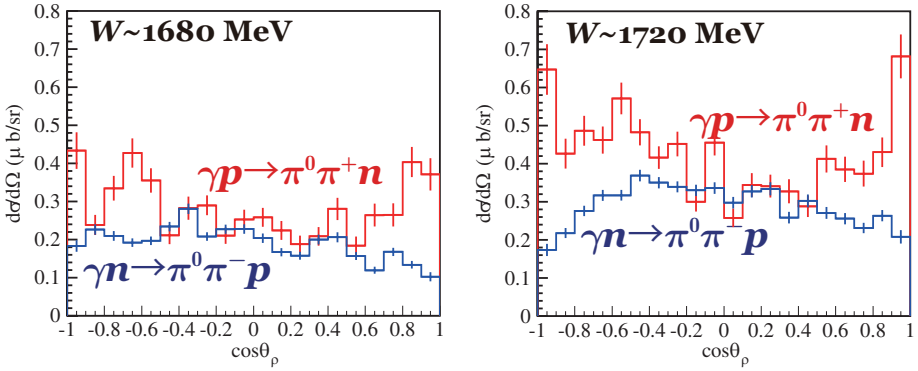

Figure 9: Differential cross section of $\rho^{\pm}$ production. Evens in which the $\pi^0\pi^{\pm}$ invariant mass is higher than 650 MeV are assumed that the $\rho^{\pm}$ meson is produced. The left panel shows that for $W \sim 1680$ MeV, and the right shows that for $W \sim 1720$ MeV. The red and blue histograms show the differential cross sections for the $\gamma p' \to \pi^0\pi^+ n$ and $\gamma n' \to \pi^0\pi^- p$ reactions.

and upward at high energies ($W_{\gamma N} \sim 1720$ MeV), respectively.

Acknowledgments

The authors express their gratitude to the ELPH accelerator staff for stable operation of the accelerators in the FOREST experiments. They are grateful to Mr. K. Matsuda, Mr. K. Nanbu, and Mr. I. Nagasawa for their technical support. This work was supported in part by the Ministry of Education, Culture, Sports, Science and Technology, Japan through Grants-in-Aid for Scientific Research (B) No. 17340063, for Specially Promoted Research No. 19002003, for Scientific Research (A) No. 24244022, for Scientific Research (C) No. 26400287, and for Scientific Research (A) No. 16H02188.

References

[1] A. Braghieri *et al.*, Phys. Lett. B **363**, 46 (1995);
W. Langgärtner *et al.*, Phys. Rev. Lett. **87**, 052001 (2001);
J. Ahrens *et al.*, Phys. Lett. B **551**, 49 (2003).

[2] T. Ishikawa *et al.*, Nucl. Instrum. Meth. A **622**, 1 (2010).

[3] T. Ishikawa *et al.*, Nucl. Instrum. Meth. A **811**, 124 (2016).

[4] F. Hinode, et al., in: Proceedings of 2005 Particle Accelerator Conference (2005) 2458.

[5] R. Hashimoto *et al.*: Research Report of LNS **41**, Tohoku University, 2009, p. 31;
H. Yamazaki *et al.*, ELPH Annual Report 2011–2013 Vol. **2–4** (2014), p. 126.

[6] T. Ishikawa *et al.*, Nucl. Instrum. Meth. A **832**, 108 (2016).

[7] S. Agostinelli, et al., Nuclear Instruments and Methods in Physics Research Section A 506 (2003) 250;
J. Allison, et al., IEEE Transactions on Nuclear Science 53 (2006) 270;
Geant4 website ⟨http://geant4.cern.ch/⟩.

[8] H. Arenhövel and A. Fix, Eur. Phys. J. A **25**, 115 (2005):
2-PION MAID web site ⟨https://maid.kph.uni-mainz.de/twopion/⟩.